J. Fluid Mech. (2004), *vol.* 510, *pp.* 29–45.
DOI: 10.1017/S0022112004009152 Printed in the United Kingdom

Drops on a conical wire

By ÉLISE LORENCEAU AND DAVID QUÉRÉ

Laboratoire de Physique de la Matière Condensée, UMR 7125 du CNRS,
Collège de France, 75231 Paris Cedex 05, France

(Received 3 June 2003 and in revised form 31 December 2003)

We study experimentally the behaviour of a drop deposited on a conical fibre. It is shown that for wetting liquids, such a drop spontaneously moves towards the region of lower curvature. The driving force is measured and shown to be a gradient of Laplace pressure, which allows us to characterize the dynamics of these self-propelling drops. We conclude by discussing the efficiency of this device for drying a solid initially coated with a liquid film.

1. Introduction

Asymmetric droplets often have the property of moving, and different ways for generating such motions have been described. Bouasse suggested that a slug in a conical capillary tube should move toward the region of small radius (Bouasse 1924). Weislogel characterized the motion of a drop deposited across the interface between two substrates of different chemical nature (Weislogel 1997). Bain, Burnett-Hall & Montgomerie (1994) and Domingues dos Santos & Ondarçuhu (1995) invented a dynamic version of that, in which the motion itself keeps alive a contrast in wettability between the front and the rear of the drop. Bico & Quéré (2002) studied the motion resulting from an asymmetric slug (made of two juxtaposed droplets) in a tube. The contrast between the rear and the front of a drop can also arise from a temperature gradient, and Brochard (1989), Smith (1995) and Mazouchi & Homsy (2000) described very completely the motion of a drop placed in a temperature gradient. Carroll (1989) focused on a drop placed on a mammalian hair fibre (which looks like a saw in profile) and noticed a tendency for it to move in a direction parallel to the fibre axis until it attains a stable conformation. This transient movement occurs as a result of differences in the local angle of contact of the liquid with the heterogeneous surface.

Generally, capillary force can be written as the product of surface tension γ and a characteristic length l. Motion can thus be induced in a drop if it is placed on a gradient of either surface tension or characteristic length – which is the case in all the examples detailed above. Here, we show what happens when a droplet is placed on a conical fibre, which achieves the situation of radius gradient. As can be observed in figure 1, the drop spontaneously moves toward the region of lower curvature. Since photographs are taken regularly (here, every 1.6 s), we also notice that the velocity is not a constant: the drop slows down as it moves. We shall see further that the drop velocity does not depend only on the conicity (i.e. gradient of radius) of the fibre, which is constant in figure 1, but also on its local radius.

This result holds at any scale below the capillary length (which compares capillary effects with gravity). It explains why atomic force microscopy tips can sometimes present self-cleaning behaviour (the end of the tip remains dry even if it has contacted a drop). This phenomenon should also be relevant in heterogeneous clusters of fibres,

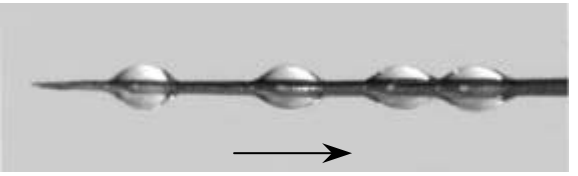

FIGURE 1. Multi-exposed photograph of a millimetric drop of silicone oil on a tapered copper wire. The time interval between two successive pictures is 1.6 s, and it is observed that the drop spontaneously moves towards the region of low curvature.

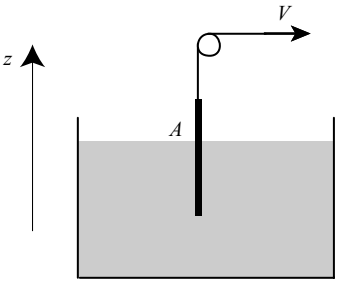

FIGURE 2. Sketch of the conical wire preparation: a copper wire is withdrawn at a constant speed V out of a bath of nitric acid.

where it should generate a reorganization of the drops (for example, displacing liquid drops from fibrous regions towards knots between fibres in glass wool, or in any non-woven fabric). It could finally be used for driving small amounts of liquid in micro-fabricated devices, or for keeping dry specific regions of such devices. In this paper, we first describe our experimental method to produce conical fibres. Then we present experimental results, and focus on the analysis of the force which drives the motion. We finally characterize the dynamics of the process and briefly consider the case of films deposited on conical fibres.

2. Construction of conical fibres

The first step of the experiment consists of making conical fibres. For a quick demonstration of the effect, we can elongate glass capillary tubes by heating and quickly drawing them. A trumpet shape results from this operation, and the effect can be easily shown – but not studied quantitatively, the shape being neither regular nor controlled. We therefore chose to develop a method using the chemical etching of a wire, as for making AFM tips (which are conical shapes of large radius gradient) (Takahashi 1990; Mononobe & Motoichi 1996; Puygranier & Dawson 2000).

A cylindrical copper wire of initial radius r_0 is vertically immersed in a bath of concentrated nitric acid (see figure 2). Then, the wire is pulled out of the bath at a controlled speed V. Nitric acid oxidizes copper, which changes the metallic atoms Cu into cations Cu^{2+}. The solution hence turns to blue. Since the wire is withdrawn, the top of the fibre spends less time in the bath than the bottom and thus is less etched by the acid. We denote as z the position along the wire, starting from the bottom. We assume that the bath is large enough to keep the concentration of the acid constant during the whole operation. During a time $\mathrm{d}t$, the nitric acid will etch a wire of radius r to a depth: $\mathrm{d}r = r(t+\mathrm{d}t) - r(t) = -v\,\mathrm{d}t$, denoting v as the speed of etching. Since

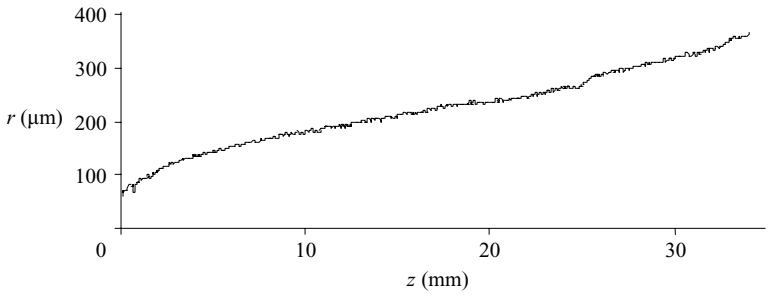

FIGURE 3. Measured mean radius r of a conical fibre as a function of the position z along the fibre.

we have $\mathrm{d}z = -V\,\mathrm{d}t$, we obtain for the variation of the radius of the wire:

$$r(z) = \frac{v}{V}z, \tag{1a}$$

taking $z = 0$ at the edge of the tip. The wire is conical, with a semi-angle α at the top given by:

$$\tan\alpha = \frac{v}{V}. \tag{1b}$$

It is possible to set the conicity α of the wire by tuning the withdrawal speed V. We also note that it should be equivalent to draw the wire once at $V/2$, or twice at V. We chose to design our conical wires by withdrawing them several times at a high speed rather than once slowly. This avoids specific effects close to the meniscus (point A in figure 2), where the chemical reaction is observed to be heterogeneous because of the presence of the liquid/vapour interface (Bico *et al.* 2004).

Figure 3 displays the profile of a conical wire of initial radius 1 mm withdrawn three times at a velocity $V = 1.5\,\mathrm{mm\,s^{-1}}$ from a bath of 60% concentrated nitric acid. High magnification digital photographs of the cone were taken and analysed, from which we could extract the contour and thus the mean radius as a function of the position z along the fibre. Except for the first few millimetres, the conicity is observed to be quite constant. Typically, the radius increases from 150 μm to 350 μm in 3 cm. Its gradient $\mathrm{d}r/\mathrm{d}z$ is found in this particular example to be $(7 \pm 1) \times 10^{-3}$, but cones with radius gradients between 4×10^{-3} and 15×10^{-3} could be produced using the same method.

3. Force measurements

3.1. *Rough data*

A drop of a wetting liquid placed on such tapered wires moves, and our first measurements consisted of determining the driving force acting on the drop. A given volume Ω of silicone oil was deposited on the wire, which was slightly inclined, as sketched in figure 4. For a given tilt angle β, we observed that the drop moves till it reaches an equilibrium position – which shows that the driving force does not depend only on α, but also on the local radius. At this point, the drop weight balances the driving capillary force, which thus provides a measurement of the latter quantity. We report in figure 5 this equilibrium position z as a function of the tilt angle, for 3 $\mathrm{mm^3}$ droplets of silicone oil (surface tension $\gamma = 19.7\,\mathrm{mN\,m^{-1}}$ and density $\rho = 910\,\mathrm{kg\,m^{-3}}$) and for the conical wire characterized in figure 3. Note that this wire is made of copper, of

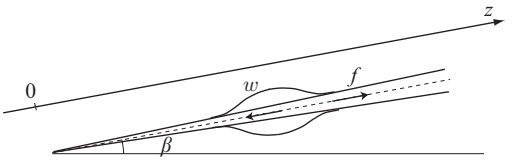

FIGURE 4. If the cone is tilted by an angle β, the drop stops at a position z for which the capillary force f balances the weight w. This experiment thus provides a measurement of the driving force acting on the drop.

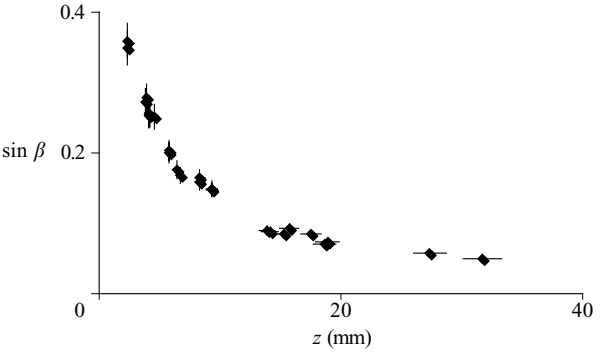

FIGURE 5. Sine of the equilibrium tilt angle β as a function of the position z of the drops on the tip. The drop, of volume 3 mm^3, is made of silicone oil ($\gamma = 19.7\,\mathrm{mN\,m^{-1}}$ and $\rho = 910\,\mathrm{kg\,m^{-3}}$).

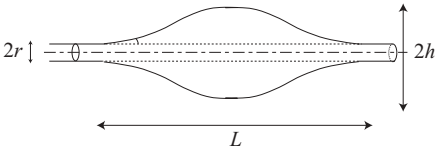

FIGURE 6. Shape of a wetting drop on a cylindrical fibre.

high surface energy, which yields a situation of total wetting. This condition will be fulfilled throughout this study.

It appears that the smaller the position z of the drop on the wire (hence the smaller the local radius r), the larger the tilt angle needed for the drop to be at rest. This shows that for a given conicity, the driving force increases as the drop becomes closer to the tip.

3.2. *Drop shape on a cylindrical fibre*

In order to be more quantitative, we must first recall different features of the shape of a drop on a cylindrical fibre, a subject on which a very comprehensive framework was built, in particular by Carroll (1976, 1983, 1986, 1991) McHale *et al.* (1997) and McHale & Newton (2002). Carroll described the equilibrium shape of small droplets (i.e. smaller than the capillary length) deposited on thin fibres (Carroll 1976, 1986). He calculated the length L, the liquid/air area A, the volume Ω and the pressure P of the drop as a function of its maximal thickness h and of the fibre radius r (as defined in figure 6). If the drop is smaller than the capillary length, its curvature is constant (gravitational effects are negligible) and proportional to its overpressure ΔP,

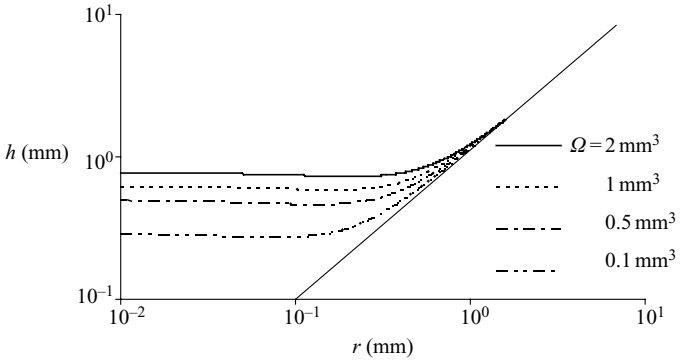

FIGURE 7. Maximum height h of a drop on a fibre, as a function of the fibre radius, for various drop volumes (increasing from bottom to top). For large radii, h tends towards r ($h = r$ is the oblique line), indicating a flattening of the drop.

according to Laplace's law. Carroll showed that this law can be expressed analytically as (Carroll 1976):

$$\Delta \mathrm{P} = \frac{2\gamma}{r+h}. \tag{2}$$

This formula is consistent with the geometry of a fibre: when the volume of the drop tends to zero (i.e. $h = r$), ΔP is equal to γ/r, the Laplace pressure inside a cylinder of radius r. On the other hand, if the radius of the fibre tends to zero for a drop of given volume, we find $\Delta P = 2\gamma/h$, the overpressure in a sphere of radius h. Furthermore, we shall use Carroll's analytical results on conical fibres: the gradient of curvature being smaller than 10^{-2}, we can neglect its effect on the shape of the drop.

In contrast with the case of a cylindrical fibre, for which the pressure inside a drop is a constant, the radius gradient along a conical fibre sets a pressure gradient along the drop. (This is easy to realize when considering a very thin drop, for which h tends to r; then, the Laplace pressure, which is γ/r, decreases towards regions of lower curvature.) According to (2), this pressure gradient along the axis of the fibre can be written as:

$$\left.\frac{\mathrm{d}P}{\mathrm{d}z}\right|_{\Omega} = -\frac{2\gamma}{(r+h)^2}\left(\frac{\mathrm{d}r}{\mathrm{d}z} + \frac{\mathrm{d}h}{\mathrm{d}z}\right)_{\Omega}, \tag{3}$$

where the subscript reminds us that the derivatives are evaluated keeping the volume Ω constant.

In order to evaluate the pressure gradient along the drop, it is necessary to know how, for a drop of given volume, the height h varies as a function of the radius r. Expressing that the pressure is constant in the drop, and writing the appropriate boundary conditions (as proposed by Carroll; see the Appendix for details), allows us to evaluate the gradient $\mathrm{d}h/\mathrm{d}r$. The corresponding results are displayed in figure 7. For each volume, two well-cut regimes can be observed. At small radius r, h is observed to become constant. The fibre hardly deforms the drop, which is nearly spherical (Joanny 1985). We thus expect $h \approx R_0$, (with R_0 the volume of the drop to be deposited: $\Omega = 4\pi R_0^3/3$), which indeed corresponds to the plateau value (note in particular in figure 7 that it increases with the drop volume). At large r, h is found to tend towards r (the equation of the oblique straight line in figure 7 is $h = r$). In this limit, the drop is expected to be very flat (quasi-cylindrical drop). The transition

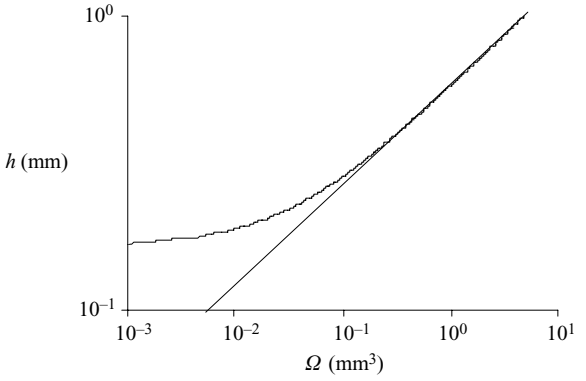

FIGURE 8. Calculated maximum height of a drop deposited on a fibre of (given) radius $r = 150\,\mu$m, as a function of the volume of the drop. The oblique line indicates the slope 1/3.

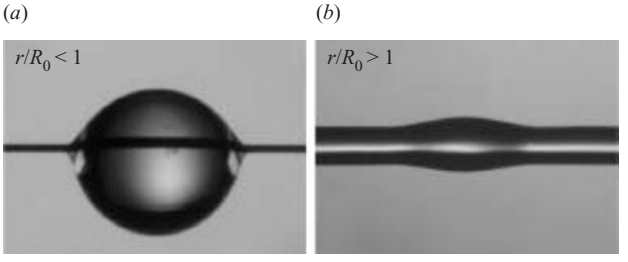

FIGURE 9. Drop of silicone oil (radius R_0) on a fibre (radius r), in the limits (*a*) $r < R_0$ and (*b*) $r > R_0$. (*a*) $R_0 = 200\,\mu$m and $r = 12\,\mu$m; (*b*) $R_0 = 80\,\mu$m and $r = 100\,\mu$m.

between these two regimes takes place for a fibre radius of the order of the drop size R_0, and thus increases with the drop volume.

This discussion can be confirmed by plotting the calculated height h as a function of the drop volume (for a fibre of a given radius) (figure 8), and illustrated by photographs (figure 9). In figure 8, we indeed note that for large drops ($\Omega > r^3$), h increases with the drop volume, as $\Omega^{1/3}$ (drawn with a straight line). This corresponds to the plateau regime in figure 7, and can be observed in figure 9(*a*). For smaller Ω, the height tends towards a plateau, which was found in figure 7 to obey the equation $h = r$: this is the flattened drop expected from our discussion, and photographed in figure 9(*b*). Although the actual unduloidal shape of a wetting drop on a fibre is complicated (Caroll 1986; McHale & Newton 2002), it is important to stress these simple asymptotic pictures (spherical and cylindrical drops), which will allow us to derive analytical results.

3.3. *Force driving a drop on a conical fibre*

We can now derive an expression for the force driving a drop on a conical fibre, in both regimes. For quasi-spherical drops ($r < R_0$), h is close to being constant (equal to R_0), and (3) simplifies into:

$$\left.\frac{\mathrm{d}P}{\mathrm{d}z}\right|_{\Omega} = -\frac{2\gamma}{(r+R_0)^2}\alpha, \tag{4}$$

where the local mean radius of the fibre is denoted as r, and the cone hemi-angle as α ($\alpha \ll 1$). Equating this gradient of capillary pressure with the gradient of gravitational

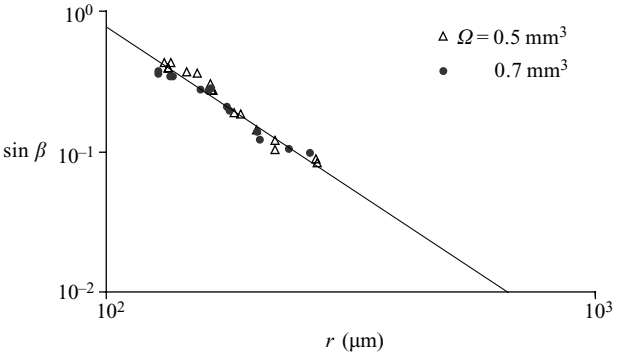

FIGURE 10. Sine of the equilibrium tilt angle as a function of the local radius of the fibre, for two (small) drop volumes. The line indicates a slope of −2.

pressure $\rho g \sin\beta$ yields an expression for the equilibrium tilt angle (as defined in figure 4), as a function of the mean radius of the fibre and its conicity:

$$\sin\beta = \frac{2\kappa^{-2}}{(r+R_0)^2}\alpha, \tag{5}$$

where the capillary length $\kappa^{-1} = \sqrt{\gamma/\rho g}$ was introduced.

For thin drops ($r > R_0$), the situation is even simpler. Making $h = r$ in (3) yields as a pressure gradient driving the motion:

$$\left.\frac{\mathrm{d}P}{\mathrm{d}z}\right|_{\Omega} = -\frac{\gamma}{r^2}\alpha. \tag{6}$$

Equation (6) can be directly derived by expressing the Laplace pressure difference between the rear and the front of the drop (of length L), namely $\gamma\alpha L/r^2$, whose gradient is indeed given by (6). Balancing this expression with gravity gives the equilibrium tilt angle in this regime of flat drops:

$$\sin\beta = \frac{\kappa^{-2}}{r^2}\alpha. \tag{7}$$

Both equations (5) and (7) are in qualitative agreement with the data displayed in figure 5; the equilibrium tilt angle quickly decreases with the position of the drop on the fibre (starting from the tip), i.e. as the fibre radius increases. This explains, in particular, our observation that decreasing the tilt angle of the conical fibre makes the drops move upwards, until it reaches the position (i.e. the mean radius) for which equilibrium between the capillary force and the weight becomes possible.

Finally we can check the model more quantitatively. In figure 10, we plotted the equilibrium tilt angle β as a function of the (measured) local radius r where the drop stays, in the limit of small volumes. The data collapse onto the same curve in a log/log scale. They are fitted well by a power law of exponent minus two, in agreement with (7). The coefficient deduced from the fit is $7000 \pm 1000\,\mu\mathrm{m}^2$, of the order of magnitude expected from (7) which provides $14\,000 \pm 2000\,\mu\mathrm{m}^2$ for this coefficient (the uncertainty coming here from the error bar on α). We also tested our model for larger drops. Corresponding data are collected in figure 11, where the equilibrium tilt angle β is plotted as a function of the (measured) quantity $r + R_0$, as suggested by (5).

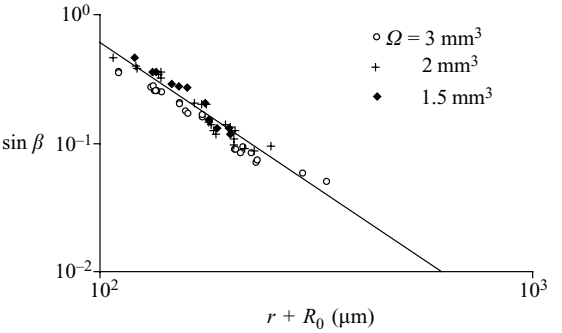

FIGURE 11. Sine of the equilibrium tilt angle β as a function of $r + R_0$, denoting r as the local radius of the fibre and R_0 as the drop radius. The line indicates a slope of -2.

There again, the representation allows us to make the different data collapse on the same curve. The scaling law predicted by the model, (5), is found to agree quite well with the data. On the other hand, the coefficient deduced from the fit, namely $5500 \pm 1500\,\mu m^2$, underestimates the one which can be deduced from (5) ($28\,000 \pm 4000\,\mu m^2$). There may be different causes for this discrepancy:

(i) We are not here fully in the limit of very large drops (for the data in figure 11, R_0 is between 700 μm and 900 μm, while r can be as large as 150 μm). As seen above, taking into account the finite size of the drop makes the numerical coefficient decrease by a factor 2 (see (5) and (7)).

(ii) The regimes described by (5) and (7) are not necessarily well defined: for a drop of given volume, decreasing β makes the drop move towards a region of higher radius (until equilibrium is reached), which makes the ratio r/R_0 change.

(iii) For the largest drops, the implicit condition $R_0 < \kappa^{-1}$ is not necessarily fulfilled, so that corrections should be introduced for taking into account the asymmetry that gravity induces on the drop shape.

4. Dynamics of the motion

4.1. *Rough data*

In this section, we consider the dynamics of droplets self-propelling on a horizontal conical fibre. The experiment consisted of placing drops of various volumes (0.2–1 mm^3) and viscosities (5–100 mPa s) on copper conical fibres (of mean radii r of the order of 150 μm) and measuring their position along the motion, from which we could deduce the drop speed as it progresses. We report such data in figure 12, for a conical fibre of gradient of curvature of about 7×10^{-3} and drops of silicone oil (of viscosity $\eta = 5$ mPa s) of various volumes.

The speed of the drop decreases as the liquid moves. For a given position on the fibre, it is also found to increase with the drop volume. All these features reveal a non-trivial dynamic, which deserves a detailed discussion. The first step is to identify the viscous force opposing the motion, and we chose to characterize this friction by studying separately the dynamics of a drop placed on a slightly inclined cylindrical fibre. This device allows us to control the driving force, the drop being set in motion under the action of its own weight.

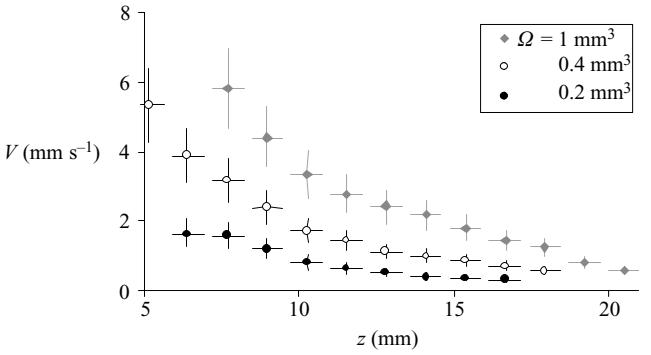

FIGURE 12. Speed of drops of different volumes as a function of their position along a conical fibre. All the drops are made of silicone oil of viscosity $\eta = 5$ mPa s.

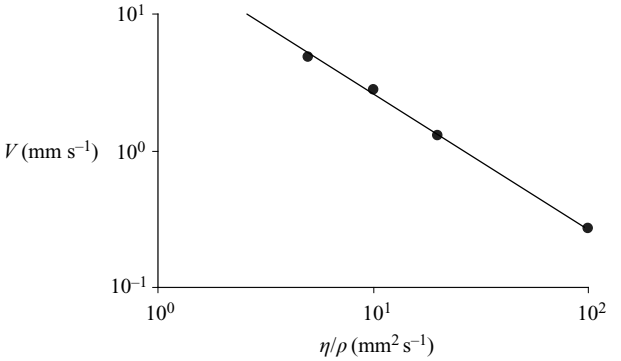

FIGURE 13. Terminal speed of oil drops placed on an inclined fibre as a function of the kinematic viscosity of the oil. The drops are made with silicone oil of various viscosities (5 mPa s $< \eta <$ 100 mPa s), and all have the same volume $\Omega = 0.6$ mm^3. The tilt angle is 7°.

4.2. *Velocity of a drop creeping down an inclined fibre*

Our first experiment here consisted of characterizing, for a given known driving force, the influence of viscosity on the dissipation. We took a cylindrical fibre, of radius $r = 100\,\mu$m, and tilted it by an angle $\beta = 7°$. Then, we measured the terminal speed V of drops (made of silicone oil of various viscosities, and of constant volume $\Omega = 0.6$ mm^3) placed on this fibre. We report our results in figure 13 as a function of the kinematic viscosity η/ρ of the oil, in a log/log scale. The terminal velocity is found to decrease with the viscosity in a log/log scale with a slope of -1, a typical feature in a viscous dissipation process. This can be confirmed considering the typical Reynolds number Re of the flow, taking R_0 as a characteristic length (note that R_0 is the largest typical length of the system). For oil viscosity increasing from 5 mPa s to 100 mPa s, we obtain a Reynolds number decreasing from 0.8 to 2×10^{-3}, always smaller than unity.

Then, we should determine the mechanism of viscous dissipation in the drop. In many cases, it is observed that the friction for a moving drop arises mainly from what happens close to the contact line, in the so-called liquid wedge. Denoting θ as the wedge angle, the dissipation is obtained by integrating the viscous stress $\eta V/\theta x$ (if x is the distance from the edge, θx is the local thickness of liquid) in the wedge. This yields $\eta V r l/\theta$, where l is a logarithmic factor including the cutoffs in the integration

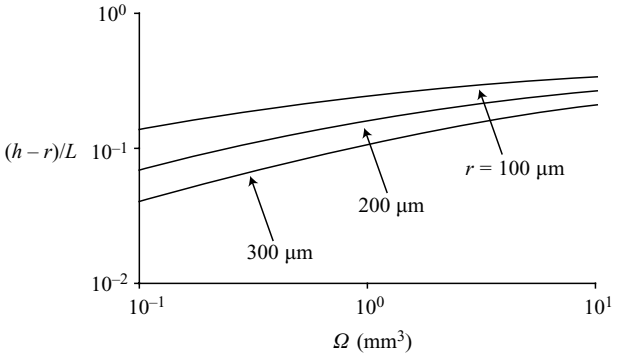

FIGURE 14. Calculated aspect ratio $(h-r)/L$ of a drop deposited on a fibre as a function of its volume.

and which can often be treated as a constant (De Gennes 1986). Hoffman showed that this logarithmic factor l is of order the of 15 (Hoffman 1975) for a liquid spreading on a dry surface, but it is reduced to a value of about 5 if the solid is prewetted by a micrometric film (Bico & Quéré 2001). The latter case indeed implies a reduction of the friction (the wedge slips on a film), and will correspond to our experiments.

For a wetting drop moving on a fibre (instead of a planar solid), the drop may itself be sketched as a global macroscopic wedge, even close to equilibrium (figures 6 and 9*b*). Hence, the total viscous resistance is the sum of two terms (the friction in a local Hoffman wedge, and that in this global macroscopic wedge), and it is not obvious to guess *a priori* which part of the drop dominates the friction. If the viscous dissipation is mainly local and for a wetting liquid, θ is dynamic in essence and given by Tanner's law (Hoffman 1975; Tanner 1979): $\theta \sim (l\eta V/\gamma)^{1/3}$. Balancing the viscous friction with the driving force f yields as an expression for the drop velocity:

$$V \sim \frac{\gamma}{\eta l}\left(\frac{f}{\gamma r}\right)^{3/2}. \tag{8}$$

If the viscous dissipation is global and assuming that the slow motion does not affect the static shape of the drop, θ is of the order of $(h-r)/L$, where the different lengths are defined in figure 2. Hence, we obtain for the velocity:

$$V \sim \left(\frac{h-r}{L}\right)\frac{f}{\eta r l}. \tag{9}$$

The dissipations are equal when the velocity is given by the relation:

$$V_c \sim \frac{\gamma}{\eta l}\left(\frac{h-r}{L}\right)^3. \tag{10}$$

If the speed V is larger than V_c, the dissipation is global, whereas it is local in the opposite case. To be more explicit, we must evaluate the ratio $(h-r)/L$, which can be done using Carroll's method (Carroll 1976, 1986). The result of the calculation is presented in figure 14 as a function of the drop volume, for different fibres.

For small drops ($\Omega < 1\,\mathrm{mm}^3$), this geometrical factor (which can be sketched as the typical angle made by the drop on the fibre, and thus directly conditions the law of dissipation) logically increases with volume. For very large drops ($\Omega > r^3$), the

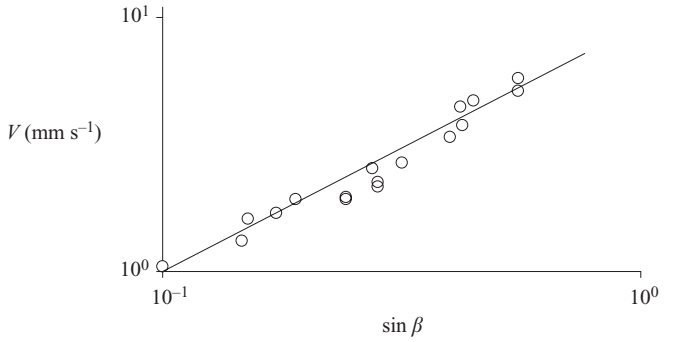

FIGURE 15. Speed of a drop of silicone oil ($\Omega = 0.5\,\mathrm{mm}^3$, $\eta = 20\,\mathrm{mPa\,s}$) running down along an inclined wire ($r = 110\,\mu\mathrm{m}$), as a function of the sine of the tilt angle. The fibre is prewetted by a film of thickness $2.0 \pm 0.5\,\mu\mathrm{m}$. The line indicates a slope of 1.

quantity $(h - r)/L$ tends towards $R_0/2R_0$, i.e. $1/2$ (as observed in figure 9*a*) and we lose the picture of a liquid wedge of small angle for the moving drop.

The velocity V_c in (10) can be estimated using figure 14: the ratio $(h - r)/L$ is found to be of the order of 0.1. The ratio γ/η is at most $5\,\mathrm{m\,s}^{-1}$, which gives (for $l = 5$) V_c less than $1\,\mathrm{mm\,s}^{-1}$, smaller than the speed of the drop placed on the wire, which suggests a global viscous dissipation, (9).

This can be tested simply by measuring the velocity of drops creeping down inclined fibres. The driving force is $f = \rho g \Omega \sin\beta$, denoting β as the tilt angle, and (8) predicts that V should increase as $\sin^{3/2}\beta$ while we expect from (9) a variation linear in $\sin\beta$. Figure 15 shows the descent velocity of a drop of silicone oil ($\Omega = 0.5\,\mathrm{mm}^3$, $\eta = 20\,\mathrm{mPa\,s}$) on a copper wire ($r = 110\,\mu\mathrm{m}$) prewetted by a thin film (thickness $2.0 \pm 0.5\,\mu\mathrm{m}$) of the same silicone oil, and inclined by an angle β, as a function of $\sin\beta$.

The speed of the drop is indeed proportional to the sine of the tilt angle, hence to the driving force, as expected from (9). The dissipation mainly occurs in the bulk rather than in the vicinity of the contact line. This is consistent with the data reported in figure 13; the speed was found to be inversely proportional to the viscosity for a constant driving force, also in agreement with (9).

Finally, we checked how the drop velocity varies as a function of its volume Ω. This is a more complicated dependency since h and L in (9) should depend on Ω. Figure 16 shows such measurements, for a given tilt angle and various viscosities, and plots the quantity $\eta V/f$ (with $f = \rho g \Omega \sin\beta$) as a function of Ω.

As expected from (9), the quantity $\eta V/f$ is not a constant, but slightly increases with the drop volume, through the geometric factor $(h - r)/L$. Describing (for convenience) the variation in figure 16 with a scaling law provides an exponent of 0.42 ± 0.05. This weak variation is in fair agreement with the results displayed in figure 14, in the range of radii and volumes explored in the experiments.

4.3. *Velocity of a drop moving along a horizontal conical wire*

We successively described the driving force of the motion ((4) or (6), according to the drop volume) and the viscous friction for a drop moving on a cylindrical fibre, (9). We can collect these results to understand the dynamics of a drop placed on a horizontal conical fibre. We shall neglect the distortion created by the gradient of curvature of the fibre (which is less than 10^{-2}) on the shape of the drop.

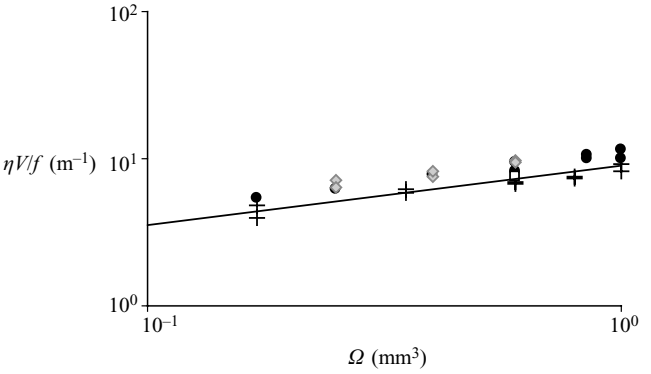

FIGURE 16. $\eta V/f$ as a function of the drop volume, for oils of different viscosities (+, $\eta = 5$ mPa s; ●, $\eta = 10$ mPa s; ◆, $\eta = 20$ mPa s; □, $\eta = 100$ mPa s) moving along the same inclined fibre ($r = 150\,\mu$m, $\beta = 7^\circ$).

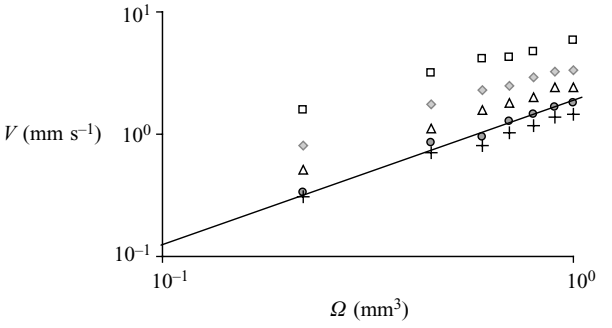

FIGURE 17. Speed of drops self-propelling on a cone (conicity $\alpha = 7 \times 10^{-3}$), as a function of the drop volume. The velocity is measured at different positions on the wire: +, $z = 17$ mm; ●, 15 mm; △, 13 mm; ◆, 10 mm; □, 8 mm. The line indicates a slope of 1.

We saw in figures 1 and 12 that the drop velocity decreases as the radius becomes larger, and increases with the drop volume. Both these facts can be understood by putting together (6) and (9) (i.e. considering the case of small drops), which yields:

$$V \sim \frac{\gamma}{\eta l}\left(\frac{h-r}{L}\right)\left(\frac{\Omega}{r^3}\right)\alpha. \tag{11}$$

Equation (11) can be tested more accurately. The first test consists of plotting the drop velocity as a function of its volume, for a given position (i.e. local radius) on the fibre. For each experiment, the fibre was first prewetted with a thin film (of typical thickness 2 μm), to prevent a drop variation along the motion: a wetting drop leaves a film behind as it moves, which leads to a decrease of its volume. Because of the prewetting, the drop volume was observed to remain constant along the motion.

The local velocity was measured and the corresponding results are displayed in figure 17, for various positions, corresponding to a variation of radius between 150 μm and 250 μm. For each position, the velocity is found to be nearly proportional to the drop volume (the thin line indicates a slope of 1 in the log–log plot of figure 17). More precisely, the quantity $(h-r)/L$ in (11) should increase slightly with the drop volume, as shown in figure 16, but this variation is very moderate in the range of radii

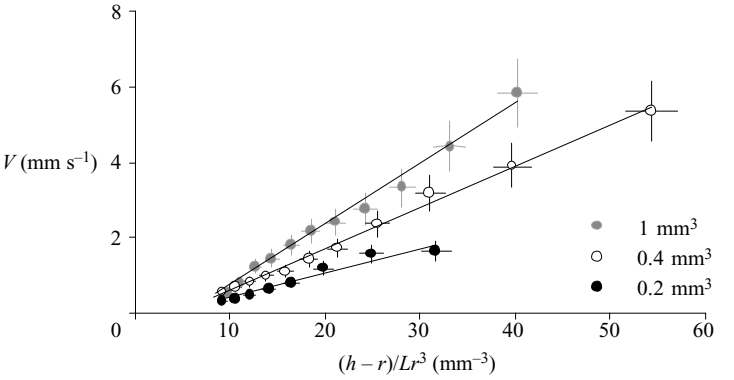

FIGURE 18. Drop speed as a function of the quantity $(h-r)/Lr^3$ for drops ($\eta = 5$ mPa s) of different volumes moving along the same conical fibre. Linear behaviours are observed, as expected from (11).

explored here (the fibre radius remains around 200 μm). This first test thus appears to be in fair agreement with (11).

However, the most remarkable feature of this dynamic law is its extreme sensitivity towards the fibre radius, which explains the rapid deceleration along the motion reported in figures 1 and 12. The quantity $(h-r)/L$ in (11) decreases with the radius of the fibre, as can be seen in figure 14 where it was displayed as a function of the drop volume for different radii. Figure 18 presents the drop velocity as a function of the quantity $(h-r)/Lr^3$, for three different volumes (where $(h-r)/L$ has been calculated using Carroll's method). There again, the results agree with (11) fairly well: in each case, a strong variation (close to r^{-4}) is observed, as predicted. This explains the deceleration along the motion, which (as we saw) is due to both a decrease of the driving force and an increase of the friction force.

5. A note on the films

In many cases, we deal with films rather than drops. This happens, for example, if a solid is drawn out of a bath, which leaves a film, or if it is exposed to a vapour which condenses on it. Here, we describe qualitatively what happens considering a film on a conical fibre, instead of a single drop. The film deposition is achieved by drawing the fibre out of bath of silicone oil at a constant velocity V_o. In such a case, the film thickness t results from a balance between viscous effects and capillarity (Quéré 1999), so that:

$$t \sim 1.34r \left(\frac{\eta V_o}{\gamma}\right)^{2/3}. \tag{12}$$

On a conical fibre, the film thickness should thus vary at each point, because of the radius variation. In our experiment, the withdrawal velocity was 1.5 cm s^{-1}, the oil viscosity and surface tension $\eta = 20$ mPa s and $\gamma = 20$ mN m^{-1}, and the fibre radius increased along the cone from, typically, 100 μm to 300 μm, which yields a film thickness varying between 8 and 25 μm. Figure 19 shows what happens once the coating is achieved.

We observe that the liquid moves to the region of smallest curvature, as reported above. However, this motion is coupled here with a destabilization of the film, because of the Plateau–Rayleigh instability (Rayleigh 1878); the film spontaneously breaks

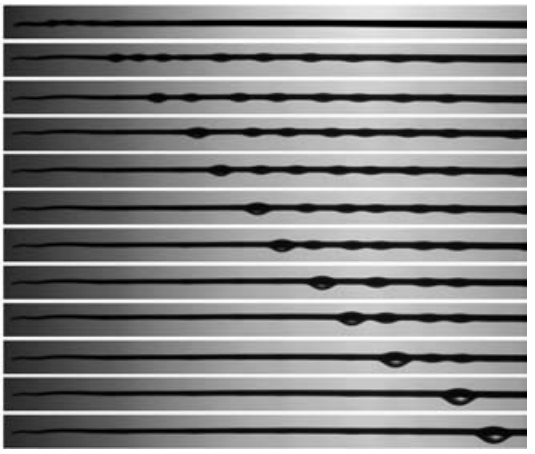

FIGURE 19. Successive snapshots (interval between each picture: 5 s) showing the evolution of a liquid film (thickness 8–25 μm) made of silicone oil ($\eta = 20$ mPa s and $\gamma = 20$ mN m^{-1}) deposited on a conical fibre (of radius between 100 and 300 μm).

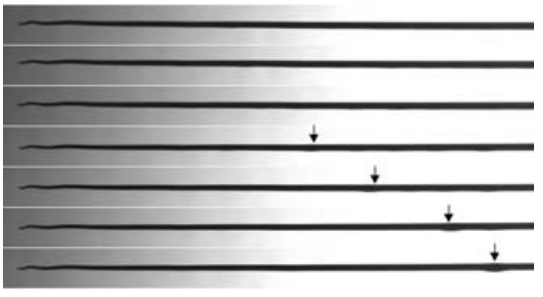

FIGURE 20. Successive snapshots (interval between each picture: 120 s) showing the evolution of a thin liquid film (thickness 2–6 μm) (same oil and fibre as in figure 19). A single drop appears and moves, as shown by the arrows.

into an array of droplets, because of the lowering of the liquid/vapour surface energy associated with the destabilization. For $t \ll r$, the wavelength of the instability scales as r, and thus the typical flow velocity for making the drops as r/τ, denoting τ as the characteristic time of the formation of the drop. τ classically comes from a balance between viscous friction, of the order of $\eta r/\tau t^2$, and capillary forces, of the order of $\gamma t/r^3$ (Dumbleton & Hermans 1970; Carroll & Lucassen 1974). This yields a time of the order of $\eta r^4/\gamma t^3$, where t is given by (12). Thus, the thinner the fibre, the smaller this time – and drops are indeed observed to appear first on the left-hand side in figure 19. The very first drop starts moving before the others and creeps quicker since it is located in the thin part of the fibre. It progressively swallows all the other droplets, which tends to make it go faster (as shown in figure 17, the drop velocity increases with the volume). This effect compensates for the slowing down due to an increase in radius, so that this drop moves at a velocity which is close to being a constant. However, the sequence displayed in figure 19 mainly shows the efficiency of this device for drying a solid region without any external action; after a while, most of the matter has been transferred towards the thickest part of the fibre.

The scenario can be slightly different if the film is thinner. Figure 20 shows the evolution of a film deposited (same oil and fibre as in figure 19) at a smaller velocity

($V_o = 0.15\,\mathrm{cm\,s^{-1}}$), which provides a film of a thickness of 2–6 μm. The main difference with the sequence displayed in figure 19 is the absence of the Rayleigh instability. However, the film is driven towards the thickest region of the fibre, as indicated by the progression (and increase in size) of a single drop. The typical velocity of the flow is given by balancing the driving gradient of capillary pressure, (6), with the viscous force (per unit volume), which scales as $\eta V/t^2$, denoting V as the mean flow velocity. This yields for the velocity:

$$V \sim \frac{\gamma}{\eta}\frac{t^2}{r^2}\alpha. \tag{13}$$

The typical time τ^* for driving the liquid on a length r thus scales as: $\eta r^3/\gamma\alpha t^2$, which means that τ^* can be smaller than the Rayleigh time τ (for setting the drops) if we have: $t < \alpha r$, i.e. for thin films. In our particular case, the thickness of the deposited film is proportional to r, (12), so that the latter condition finally corresponds to small deposition velocities. Note that the efficiency of the drying can finally be evaluated by comparing the volume of the drop which collects the film (and which can be deduced from its geometrical characteristics, as shown by Carroll 1976) with the volume of the film. Such a comparison was made for the experiments of figures 19 and 20 and showed that $85 \pm 15\%$ of the volume was collected – a quantity logically smaller than unity, because of the film deposited by the collecting drop itself, and of the microscopic film which remains stuck to the fibre in these wetting situations (Brochard 1986).

6. Conclusion

We showed in this paper that a drop of a wetting liquid placed on a conical fibre spontaneously moves towards regions of large radius. The force driving the motion was found to be a gradient of Laplace pressure, and thus be scaled by the liquid surface tension γ. This can be understood by discussing briefly the energetic origin of the motion. A drop of wetting liquid progressing on a solid (for example, spreading on it or penetrating its pores) does not modify the solid surface energy of the substrate, because of the microscopic wetting film emitted by the drop ahead of the apparent contact line (De Gennes 1985). Hence, this drop progresses on a wetted solid, and the gain of energy associated with the motion is just the lowering of the liquid/vapour interface. On a conical fibre, this lowering physically comes from the flattening of the drop as it moves towards thick regions, and from the lowering of the ratio surface/volume in these regions.

If the wetting was only partial, the discussion would be much more complex, in particular, because the possible conformations of a drop include non-axisymmetric shapes. For example, drops which are small enough can gain energy if rolling on one side of the fibre: this is the so-called roll-up process, which was described by Adam (1937), Carroll (1986) and McHale, Newton & Carroll (2001). In addition, the contact angle hysteresis generally associated with partial wetting induces a force which resists the motion, which would suppress, in most cases, the effect reported here.

Thus, we considered only wetting situations. The force acting on the drops was found to be mainly fixed by the local radius r of the fibre (since it decreases as $1/r^2$). This fact, together with an increase of the friction as the fibre becomes thicker, explains why the drops were found to slow down along their progression. This motion can be exploited for drying a solid, even if forced to be coated with a film (which can be achieved either by a relative motion between the liquid and the solid, or by exposing

the latter to a vapour which condenses on it). Films are driven towards regions of large radius, which shows that such cones could be used as efficient condensers, large surface areas being coated and 'pumped' towards thicker regions where the liquid can be collected, without using a motor.

We sincerely thank Étienne Reyssat for very stimulating discussions, and Jens Eggers for pointing out a mistake in a first version of the manuscript.

Appendix

In this Appendix, we detail how (2) is derived. At equilibrium, the free energy of a drop is minimum. The energy G we must minimize can be written:

$$G = \gamma A - \lambda \Omega,$$

where A is the liquid/air interface, γ is the liquid/air surface tension, Ω is the volume of the drop and λ is a Lagrange multiplier related to the condition of a constant volume. Denoting as z the distance from the fibre axis Ox, the free energy is equal to:

$$G = \pi \int [2z\sqrt{1+\dot{z}^2} - \lambda(z^2 - r^2)]\,\mathrm{d}x, \tag{A 1}$$

where $\dot{z}$ is $\mathrm{d}z/\mathrm{d}x$, and r is the fibre radius. We denote f the function such that $G = \int f(z, \dot{z})\,\mathrm{d}x$. As G is the extremum, the function f satisfies the Euler–Lagrange equation:

$$-\frac{\mathrm{d}}{\mathrm{d}x}\left(\frac{\partial f}{\partial \dot{z}}\right) + \frac{\partial f}{\partial z} = 0.$$

Hence, we obtain:

$$\gamma\left[\frac{-\ddot{z}}{(1+\dot{z}^2)^{3/2}} + \frac{1}{z(1+\dot{z}^2)^{1/2}}\right] = \lambda. \tag{A 2}$$

This is the Laplace equation, since the quantity inside the brackets expresses the curvature in axisymmetric coordinates. We deduce that

$$\lambda = \Delta P.$$

The Lagrange multiplier is equal to the pressure inside the drop. Moreover, (A 2) can be integrated once:

$$-\Delta P\frac{z^2}{2} + \gamma\frac{z}{(1+\dot{z}^2)^{1/2}} = K,$$

where K is a constant that can be evaluated using the boundary condition: $\dot{z} = 0$ when $z = r$ (the liquid wets the solid). Therefore, it becomes:

$$-\Delta P\frac{z^2 - r^2}{2} + \gamma\left(\frac{z}{(1+\dot{z}^2)^{1/2}} - r\right) = 0.$$

A second integration can be performed with the condition $\dot{z} = 0$ for $z = h$. Hence, we find that

$$\Delta P = \frac{2\gamma}{r+h}, \tag{A 3}$$

which is (2). Note, finally, that (A 2) together with (A 3) and the appropriate boundary conditions ($\dot{z} = 0$ when $z = r$ and $z = h$) allows us to compute all the characteristics of the drop, such as its length and surface area, as shown by Carroll (1976, 1986).

REFERENCES

Adam, N. K. 1937 Detergent action and its relation to wetting and emulsification. *J. Soc. Dyers Colour*. **53**, 122–129.

Bain, C., Burnett-Hall, G. & Montgomerie, R. 1994 Rapid motion of liquid drops. *Nature (Lond.)* **372**, 414–415.

Bico, J. & Quéré, D. 2001 Falling slugs. *J. Colloid Interface Sci.* **243**, 262–264.

Bico, J. & Quéré, D. 2002 Self-propelling slugs. *J. Fluid Mech.* **467**, 101–127.

Bico, J., Vierling, J., Vigano, A. & Quéré, D. 2004 Self-similar etching. *J. Colloid Interface Sci.* **270**, 247–249.

Bouasse, H. 1924 *Capillarité, phénomènes superficiels*. Delagrave, Paris.

Brochard, F. 1986 Spreading of liquid drops on thin cylinders: the 'manchon/droplet' transition. *J. Chem. Phys.* **84**, 4664–4672.

Brochard, F. 1989 Motions of droplets on solid surfaces induced by chemical or thermal gradients. *Langmuir* **5**, 432–438.

Carroll, B. J. & Lucassen, J. 1974 Effect of surface dynamics on the process of droplet formation from supported and free liquid cylinders. *J. Chem. Soc. Faraday Trans.* **70**, 1228–1239.

Carroll, B. J. 1976 The accurate measurement of contact angle, phase contact areas, drop volume, and Laplace excess pressure in drop on fiber system. *J. Colloid Interface Sci.* **57**, 488–495.

Carroll, B. J. 1983 The equilibrium of liquid drops on smooth and rough circular cylinders. *J. Colloid Interface Sci.* **97**, 195–200.

Carroll, B. J. 1986 Equilibrium conformation of liquid drops on thin cylinders under forces of capillarity. A theory for the roll-up process. *Langmuir* **2**, 248–250.

Carroll, B. J. 1989 Droplet formation and contact angles of liquids on mammalian hair fibres. *J. Chem. Soc. Faraday Trans.* 1 **85**, 3853–3860.

Carroll, B. J. 1991 Comment on 'Spreading of liquid droplets on cyclindrical surfaces: accurate determination of contact angle.' *J. Appl. Phys.* **70**, 493–494.

De Gennes, P. G. 1985 Wetting: statics and dynamics. *Rev. Mod. Phys.* **57**, 827–863.

De Gennes, P. G. 1986 Deposition of a Langmuir–Blodgett layers. *Colloid Polymer Sci.* **264**, 463–465.

Domigues dos Santos, F. & Ondarçuhu, T. 1995 Free running droplets. *Phys. Rev. Lett.* **75**, 2972–2976.

Dumbleton, J. H. & Hermans, J. J. 1970 Capillary instability of a thin annular layer of liquid around a solid cylinder. *Indust. Engng Chem. Fundam.* **9**, 466–469.

Hoffman, R. 1975 A study of the advancing interface. *J. Colloid Interface Sci.* **50**, 228–241.

Joanny, J. F. 1985 Le mouillage. PhD thesis, University of Paris 6.

McHale, G., Käb, N. A., Newton, M. I. & Rowan, S. M. 1997 Wetting of a high-energy fiber surface. *J. Colloid Interface Sci.* **186**, 453–461.

McHale, G., Newton, M. I. & Carroll, B. J. 2001 The shape and stability of small liquid drops on fibers. *Oil Gas Sci. Technol.* **56**, 47–54.

McHale, G. & Newton, M. I. 2002 Global geometry and the equilibrium shapes of liquid drops on fibers. *Colloids Surfaces* A **206**, 79–86.

Mazouchi, A. & Homsy, G. M. 2000 Thermocapillary migration of long bubbles in cylindrical capillary tubes. *Phys. Fluids* **12**, 542–549.

Mononobe, S. & Motoichi, O. 1996 Fabrication of a pencil-shaped fiber probe for near-fields optics by selective chemical etching. *J. Lightwave Technol.* **14**, 2231–2235.

Puygranier, B. A. F. & Dawson, P. 2000 Chemical etching of optical fibre tips-experiment and model. *Ultramicroscopy* **85**, 235–248.

Quéré, D. 1999 Fluid coating on a fiber. *Annu. Rev. Fluid Mech.* **31**, 347–384.

Rayleigh, Lord 1878 On the instability of jets. *Proc. R. Soc.* **10**, 4–13.

Smith, M. K. 1995 Thermocapillary migration of a two-dimensionnal liquid droplet on a solid surface. *J. Fluid Mech.* **294**, 209–230.

Takahashi, K. M. 1990 Meniscus shape on small diameter fibers. *J. Colloid Interface Sci.* **134**, 181–187.

Tanner, L. H. 1979 The spreading of silicone oil drops on horizontal surfaces. *J. Phys.* D: *Appl. Phys.* **12**, 1473–1484.

Weislogel, M. M. 1997 Steady spontaneous capillary flow in partially coated tubes. *AIChE J.* **43**, 645–665.